Potential impact of changes in river nutrient supply on global ocean biogeochemistry

Leticia Cotrim da Cunha,[1,2] Erik T. Buitenhuis,[1,3] Corinne Le Quéré,[1,3,4] Xavier Giraud,[1,5] and Wolfgang Ludwig[6]

Received 14 March 2006; revised 5 July 2007; accepted 24 July 2007; published 24 October 2007.

[1] The growing world population increases the demand for water, energy, and land. This demand for natural resources impacts the transport of material and the supply of nutrients in the coastal ocean by rivers. We assess the potential impact of river N, Si, Fe, and organic carbon (OC) fluxes on the global and coastal ocean biogeochemistry, using an ocean biogeochemistry model and observations, in eight different scenarios. We assess two extreme scenarios, one with no river nutrients, corresponding to a complete stop of nutrient input by rivers, and one with high nutrient fluxes, corresponding to a world population of 12 billion people. Compared to today's scenario values, primary production (PP) changes from −5% to +5% for the open ocean, and from −16% to +5% for the coastal ocean. In the coastal ocean the impact of river nutrients on PP depends on regional nutrient limitation. River inputs have a larger impact on PP in areas where upwelling and high runoff are combined. The coastal ocean is typically N- or Si-limited. River Fe not assimilated by the phytoplankton is exported to open ocean areas, and its fertilizing effect depletes coastal and open ocean surface waters from N and Si. The impact on PP is reflected on global ocean low-O_2 areas whose extent changes from −16% to +23% across the range of scenarios. River nutrients have a modest impact on the global ocean CO_2 sink of up to 0.4 Pg C a^{-1}, depending on the amount of inorganic and organic carbon transported by the rivers.

Citation: Cotrim da Cunha, L., E. T. Buitenhuis, C. Le Quéré, X. Giraud, and W. Ludwig (2007), Potential impact of changes in river nutrient supply on global ocean biogeochemistry, *Global Biogeochem. Cycles*, *21*, GB4007, doi:10.1029/2006GB002718.

1. Introduction

[2] Rivers can have a significant impact on the hydrography and biogeochemistry of ocean areas. Evaluation of the impact of river-transported nutrients and carbon within the coastal and global ocean has been hindered in the past by the lack of global estimates of the river nutrient discharges. One of the global issues of the impacts on fluvial systems is that it affects the coastal ocean biogeochemistry by the input of nutrients [*Meybeck*, 1998] over short timescale. Over geological timescales, river fluxes of materials have an influence on seawater composition [*Liu et al.*, 2000]. Nutrients are delivered through natural leaching and erosion processes in the catchments draining to the coastal ocean [*Smith et al.*, 2003].

[3] The budget of carbon and nutrients in the coastal zone determines to a large extent if this area acts as either a source or sink of atmospheric CO_2. It has been shown that the effect of riverine and other terrestrial nutrient inputs on coastal eutrophication can impact the annual global carbon budget [*Smith and Hollibaugh*, 1993] and the interhemispheric transport of carbon [*Aumont et al.*, 2001]. Additionally, the modeling study by *Mackenzie et al.* [1998] suggests that net heterotrophy over continental margins has influenced the global carbon budget over the last hundreds of years.

[4] Inputs of riverine nutrients have increased as a result of increasing human activity in the catchments. Some inputs are proportional to population density (sewage), and others are not (agricultural, atmospheric fallout) [*Smith et al.*, 2003]. Heavy nutrient loading can accelerate ecosystem metabolism and may lead to anoxia, like in the Gulf of Mexico [*Rabalais et al.*, 2002]. *Smith et al.* [2003] showed that total nutrient loads increased about three times from the 1970s (26 Gmol DIN a^{-1} and 480 Gmol DIN a^{-1}) to the 1990s (74 Gmol DIN a^{-1} and 1350 Gmol DIN a^{-1}) [*Meybeck*, 1982; *Meybeck and Ragu*, 1997].

[5] River regulation by damming may substantially reduce sediment and nutrient inputs to the ocean [*Jickells*, 1998; *Vörösmarty et al.*, 2003]. Si fluxes are also altered by

[1]Max Planck Institute for Biogeochemistry, Jena, Germany.
[2]Now at Leibniz-Institut für Meereswissenschaften, Marine Biogeochemie, Kiel, Germany.
[3]Now at School of Environmental Sciences, University of East Anglia, Norwich, UK.
[4]Also at the British Antarctic Survey, Cambridge, UK.
[5]Now at Research Center "Ocean Margins", University of Bremen, Bremen, Germany.
[6]CEFREM UMR-CNRS 5110, University of Perpignan, Perpignan, France.

0886-6236/07/2006GB002718

damming, but no compensation for Si occurs by anthropogenic activities. Damming alters the N:Si and P:Si ratio of nutrients delivered to the coastal ocean [*Humborg et al.*, 2000]. Therefore the food chain in the coastal sea, typically dominated by diatoms, which are the usual food for mesozooplankton (copepods) may be altered [*Humborg et al.*, 2000; *Justic et al.*, 1995].

[6] According to *Chen et al.* [2003], river fluxes of carbon and nutrients do not have a significant impact on the global open ocean, but can have important effects on the coastal ocean. The coastal ocean responds faster to changes in land, ocean and atmospheric nutrient fluxes [*Mackenzie et al.*, 2004]. In this paper we assess the potential global and regional impacts of river nutrient fluxes on the global and coastal ocean biogeochemistry. We discuss how river nutrients affect primary and export production, and the extent of low-oxygen areas, and how much of the export production in the coastal ocean can be sustained by river nutrient inputs. We exploit recent methods to estimate riverine inorganic and organic carbon, and nutrient loads (N, Si, and Fe), and we test simulations of different river nutrient scenarios using a global ocean biogeochemistry model. We create scenarios of increasing nutrient inputs to the coastal ocean due to population increase to gain insight on the impact of anthropogenic activity in the coastal zone.

2. Methods

2.1. Model Design

[7] We used the PISCES-T ocean biogeochemistry model [*Buitenhuis et al.*, 2006], which is a modification of the Pelagic Interactions Scheme for Carbon and Ecosystem Studies (PISCES) model developed by *Aumont et al.* [2003] and *Bopp et al.* [2003]. PISCES-T includes the representation of diatoms, nanophytoplankton, mesozooplankton, and microzooplankton. Phytoplankton growth is colimited by light and by total N, Si and Fe. For all compartments, the C:N ratio is kept constant to the values proposed by *Takahashi et al.* [1985] (122:16). PISCES-T includes O_2 and a full carbon cycle accounting for dissolved inorganic carbon (DIC), total alkalinity (TALK), $CaCO_3$, dissolved organic carbon (DOC) and 2 sizes of particulate organic carbon (POC). The remineralization rate for DOC is 0.018 d^{-1} and the degradation rate for POC is 0.18 d^{-1} [*Buitenhuis et al.*, 2006]. Nutrient limitation has a more pronounced effect on diatoms than on nanophytoplankton. This is represented in PISCES-T by increased half-saturation constants (Diatoms K_m are 0.5 μM NO_3, 4 μM SiO_3, 0.12 nM Fe, and Nanophytoplankton K_m are 0.125 μM NO_3 and 0.025 nM Fe) [*Aumont and Bopp*, 2006; *Aumont et al.*, 2003; *Bopp et al.*, 2003]. This is due to the relatively low affinity of diatoms for nutrients because of their low surface:volume ratio. The partial pressure of CO_2 at the surface (pCO_2) is computed using the modeled DIC, sea surface temperature (SST), sea surface salinity (SSS) and surface alkalinity.

[8] The model is initialized with observations in 1948, using annual mean observations when available: DIC and TALK [*Key et al.*, 2004], NO_3^{3-}, SiO_3^-, and O_2 from *Conkright et al.* [2002] and *Locarnini et al.* [2002], respectively. All other tracer fields were initialized with the steady state fields of *Aumont et al.* [2002]. Observed DIC corresponds approximately to the year 1990: It was corrected to the beginning year of the simulation in 1948 by subtracting a model estimate of the anthropogenic CO_2 absorbed during 1948–1990 [*Le Quéré et al.*, 2003]. PISCES-T uses the global monthly dust deposition maps from the *Tegen and Fung* [1995] model. Dust is considered a source of Fe and Si to the ocean. We consider that dust contains 3.5% and 30.8% of Fe and Si, respectively. However, all the iron and silica deposited to the ocean are not readily available for biology. Here we used 2% solubility for deposited iron, an intermediate value inside the range given by *Jickells and Spokes* [2001], and 7.5% solubility for silica [*Moore et al.*, 2002]. The total atmospheric Fe and Si fluxes are 166.25 Gg Fe a^{-1} (2.98 Gmol Fe a^{-1}) and 5.75 Tg Si a^{-1} (204.88 Gmol Si a^{-1}). We consider a sediment Fe input of 246.51 10^{-3} Gg Fe a^{-1} (4.41 10^{-3} Gmol Fe a^{-1}). The model includes a constant coastal Fe supply to reproduce the effect of sediment resuspension. The nutrient budgets (Si, N:P, and Fe) are closed through a compensation of inputs (atmosphere, rivers and sediments) by removing particulate and dissolved organic nutrients from the bottom water layer. Since this closure of the budget is only important to maintain the total nutrient inventory of the ocean when running the model over hundreds of years, we did not change the amounts that are removed between the different simulations (6.88 Tmol PSi a^{-1}, 2.07 Tmol DON a^{-1}, 2.77 Tmol PON a^{-1}, and 3.36 Gmol POFe a^{-1}), even though the amounts that were added were changed. This ensures that all effects that we report here can be attributed directly to changes in the river nutrient supply.

[9] PISCES-T is embedded in the OPA global circulation model [*Madec et al.*, 1999] using the ORCA2 grid. The resolution of ORCA2 is 2° longitude by on average 1.1°, with a higher-latitude resolution at the equator and at the poles (0.5°). The model represents 30 vertical levels, with 10 m resolution in the surface 100 m of the ocean. The deepest layer is 500 m thick and reaches 5000 m depth. The model time step in our version is 1 h 36′. Effects of nonresolved subgrid-scale movements are parameterized by horizontal and vertical diffusion. The horizontal diffusivity coefficient is constant everywhere at 2000 m^{-2} s^{-1} and the vertical diffusivity coefficient is computed prognostically throughout the water column, allowing the mixed layer depth to vary in time and space [*Blanke and Delecluse*, 1993]. In OPA the vertical eddy diffusivity and viscosity coefficients are calculated by a 1.5-order turbulent kinetic energy model [*Gaspar et al.*, 1990]. The eddy viscosity coefficient depends on geographical position. It is taken as 40000 m^2 s^{-1} and reduced in the equator regions (2000 m^2 s^{-1}) except near the western boundaries. Subgrid eddy induced mixing is parameterized according to *Gent and McWilliams* [1990]. The model was forced by the daily wind and water fluxes from NCEP/NCAR reanalysis [*Kalnay et al.*, 1996] from 1948 to 2005 as in *Buitenhuis et al.* [2006] and *Le Quéré et al.* [2003]. The solar radiation penetrates the top meters of the ocean. The downward irradiance is formulated with two extinction coefficients [*Paulson and Simpson*,

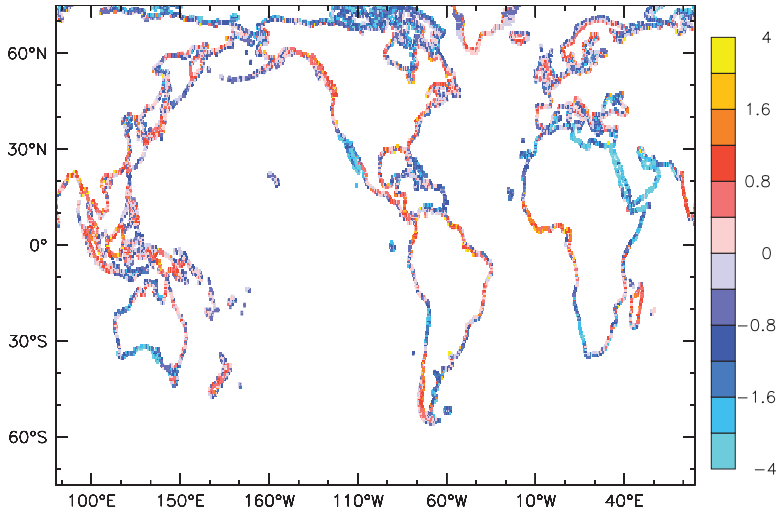

Figure 1. Annual river water runoff in $km^3\ a^{-1}$ on logarithm scale [*Korzoun et al.*, 1977; *Ludwig et al.*, 1998; *Doell and Lehner*, 2002].

1977] whose values correspond to average open ocean conditions [*Manizza et al.*, 2005].

[10] In this study, we define the coastal ocean as the areas where the maximum depth is <200 m, corresponding to 3×10^{13} m^2 (8% of global ocean area) in the ORCA grid. Because of its coarse resolution the model is unable to represent details of coastal areas and circulation. Higher model resolution would improve the results from our simulations.

[11] We ran the model from 1948 to 1992 as in *Carr et al.* [2006] and *McKinley et al.* [2006]. This is long enough for the surface ocean to approximate steady state, as shown by the stability of the results after 3–4 a of simulations. Then we did several simulations of 13-a from 1993 to 2005 with the PISCES-T model considering different riverine nutrient load estimates. We present average output for years 1998–2005.

2.2. Estimation of River Nutrient Input

[12] Annual fluxes of riverine carbon and nutrient (N, Si, Fe) to the ocean were computed following a global river drainage direction map (DDM30), considering population and basin area [*Doell and Lehner*, 2002], and river runoff [*Korzoun et al.*, 1977; *Ludwig et al.*, 1998] at 0.5° increments of latitude and longitude. This map represents the drainage directions of surface water on all continents, except Antarctica. Cells of the map are connected by their drainage directions and are thus organized into drainage basins. In this work we used the cells corresponding to basin outlets to the ocean as input data for our simulations (Figure 1).

2.2.1. Dissolved Inorganic Nitrogen (DIN)

[13] To calculate riverine DIN inputs we used a regression model originally developed by *Smith et al.* [2003] (equation (1)). The model describes DIN export by the analysis of 165 systems for which DIN flux data is available [*Meybeck and Ragu*, 1997; S. Smith and F. Wulff (Eds.), LOICZ-Biogeochemical modelling node, 2000, available at http://data.ecology.su.se/MNODE/]. In this model, riverine DIN export to the coastal zone is a function of basin population density and runoff:

$$\log DIN = 3.99 + 0.35 \times \log POP + 0.75 \times \log R \qquad (1)$$

where (DIN) is in mol N $km^{-2}\ a^{-1}$, (POP) is population density in people km^{-2}, and (R) is runoff in m a^{-1}. On the basis of basin area, basin population (for the year 1990) and runoff provided by the DDM30 map, 16.3 Tg DIN a^{-1} (1.16 Tmol N a^{-1}) are transported to the coastal zone by rivers. In the *Smith et al.* [2003] model, the average N:P ratio of riverine export is 18:1, which is close to the PISCES-T N:P ratio of 16:1. Nitrogen retention in estuarine areas was not included owing to lack of global data. Our estimate is similar to other published values [*Green et al.*, 2004; *Seitzinger et al.*, 2002; *Smith et al.*, 2003] but lower than the recent estimate of 25 Tg DIN a^{-1} [*Dumont et al.*, 2005].

[14] We used the future population scenario from the United Nations Population Division [*UNPD*, 2004] of 12×10^9 inhabitants for 2050 to recalculate the DIN input using equation (1). This strategy was previously used by *Seitzinger et al.* [2002] to estimate nitrogen input by rivers to the coastal area, considering population density and land use. Compared to *Seitzinger et al.*'s [2002] DIN estimates for 2050, our "future average" N:P ratio of riverine export increased to 30:1. This difference is explained by the explicit representation of agricultural N inputs in *Seitzinger et al.* [2002]. Thus to adjust this increase in N inputs we multiplied our DIN "HIGH_N" scenario values by (30/18). The DIN inputs were recalculated considering 12×10^9 inhabitants for 2050.

2.2.2. Dissolved Silica (Si)

[15] Rivers are responsible for 80% of the inputs of Si to the ocean [*Treguer et al.*, 1995]. For an estimate of riverine input of dissolved Si we used the runoff data from the DDM30 map, and applied an average concentration of Si in river waters of 4.2 mg Si L^{-1} [*Treguer et al.*, 1995]. Si

Table 1. River Nutrient Scenarios

Scenario Name	Riverine Inputs: OM, T mol C a^{-1}	IC, T mol C a^{-1}	N, T mol a^{-1}	Si, T mol a^{-1}	Fe, G mol a^{-1}	Details on Riverine Nutrient Inputs
NO_RIVER	0	0	0	0	0	no riverine nutrients
RDIC	0	32.1	0	0	0	DIC[a]
RDOC	15.8	0	2.1	0	0.079	DOM[a]
RPOC	12.3	0	1.6	0	0.062	POM[a]
RF99	0	0	0	0	0.32	Fe (99% loss)[b]
RSIL	0	0	0	6.7	0	Si[c]
RNIT	0	0	1.2	0	0	DIN[d]
TODAY	28.1	32.1	4.9	6.7	0.46	DIN[d], Si[c], Fe (99% loss)[b], DIC[a], DOM[a], POM[a]
TODAY_HiF[e]	28.1	32.1	4.9	6.7	6.64	DIN[d], Si[c], high Fe (80% loss)[f], DIC[a], DOM[a], POM[a]
HIGH_N	28.1	32.1	7.1	6.7	6.64	High DIN[e], Si[c], high Fe (80% loss)[f], DIC[a], DOM[a], POM[a]

[a][*Doell and Lehner*, 2002; *Ludwig et al.*, 1996a; *Ludwig et al.*, 1996b].
[b][*Chester*, 1990; *Doell and Lehner*, 2002; *Martin and Meybeck*, 1979], 1% net Fe flux to the ocean.
[c][*Doell and Lehner*, 2002; *Treguer et al.*, 1995].
[d](Population = 6×10^9 inh.) [*Doell and Lehner*, 2002; *Smith et al.*, 2003; *UNPD*, 2004].
[e](Population = 12×10^9 inh.) [*Doell and Lehner*, 2002; *Smith et al.*, 2003; *UNPD*, 2004].
[f][*Chester*, 1990; *Doell and Lehner*, 2002; *Martin and Meybeck*, 1979], 20% net Fe flux to the ocean.

concentration in river water is variable according to basin geology but regional data is not available. Our estimate leads to a dissolved Si river input of 187 Tg Si a^{-1} to the ocean. This value is comparable to the range of 140 ± 30 Tg Si a^{-1} for a net riverine dissolved Si input to the ocean proposed by *Treguer et al.* [1995], considering estuarine retention of Si.

2.2.3. Dissolved Iron (Fe)

[16] Iron plays a crucial role in ocean biogeochemistry. Rivers and continental shelf sediments supply Fe to surface waters. Because it is extensively removed from the dissolved phase in estuaries, rivers are thought to be a minor source for the open ocean, but not for coastal zones. We used the runoff data from the DDM30 map and applied an average concentration of dissolved Fe in river waters of 40 μg L^{-1} [*Martin and Meybeck*, 1979; *Martin and Whitfield*, 1983]. As for Si, river basin geology influences Fe concentration in river water, but there is no available global database on riverine Fe. Our estimate leads to a gross dissolved Fe input of 1.75 Tg Fe a^{-1}, comparable to the estimate of 1.45 Tg Fe a^{-1} by *Chester* [1990]. During estuarine mixing, flocculation of colloidal Fe and organic matter forms particulate Fe because of the major change in ionic strength upon mixing of fresh water and seawater [*de Baar and De Jong*, 2001]. This removal has been well documented in many estuaries. Literature values show that approximately 80 to 99% of the gross dissolved Fe input is lost to the particulate phase in estuaries at low salinities [*Boyle et al.*, 1977; *Chester*, 1990; *Dai and Martin*, 1995; *Lohan and Bruland*, 2006; *Sholkovitz*, 1978]. We applied the removal rates of 80% and 99% to our gross Fe flux, and obtained a net input of riverine dissolved Fe to the coastal ocean of 0.35 and 0.02 Tg Fe a^{-1}, respectively.

2.2.4. Particulate (POC) and Dissolved Organic (DOC) and Inorganic (DIC) Carbon

[17] The predicted river carbon fluxes are based on models relating river carbon fluxes to their major controlling factors [*Ludwig and Probst*, 1998; *Ludwig et al.*, 1996b]. For POC, sediment flux is the dominant controlling parameter. For DOC, runoff intensity, basin slope, and the amount of soil OC in the basin are the controlling parameters [*Ludwig et al.*, 1996b]. We applied this model to the DDM30 data set, and we estimate a gross discharge of 148 Tg C a^{-1} and 189 Tg C a^{-1} for POC and DOC, respectively. We assume that DOC has a conservative behavior in estuaries. These values are in agreement with recent modeled values of 170 Tg C a^{-1} as DOC [*Harrison et al.*, 2005], and 197 Tg C a^{-1} as POC [*Beusen et al.*, 2005; *Seitzinger et al.*, 2005]. We used a C:N:Fe ratio of 122:16:6.1 $\times$ 10^{-4}, thus riverine DOC and POC, when they are remineralized, are also N and Fe sources to the ocean (Table 1). Inorganic carbon is mainly transported by rivers in the dissolved form. For DIC inputs, drainage intensity and river basin lithology are the controlling parameters [*Ludwig et al.*, 1996a]. We applied this model to the DDM30 data set, and we estimate a DIC discharge of 385 Tg C a^{-1} (32.12 Tmol C a^{-1}).

2.3. Experimental Scenarios

[18] We considered two extreme scenarios, one without river nutrients, and one with high loads of Fe, and DIN according to the population scenario for 2050. Additionally, we use eight scenarios to assess the impacts of "single" river inputs on biogeochemistry (Table 1):

[19] 1. NO_RIVER: no river nutrient supply. It represents an extreme situation where river nutrient fluxes would stop completely. We do not consider a reduction in freshwater input to the ocean.

[20] 2. RDIC: This scenario considers riverine DIC fluxes.

[21] 3. RDOC: This scenario considers riverine DOC inputs. Riverine DOC has the same turnover time as marine DOC.

[22] 4. RPOC: This scenario considers riverine POC inputs. Riverine POC has the same turnover time as marine POC_{small}.

[23] 5. RNIT: This scenario considers riverine DIN fluxes, calculated for today's world population.

[24] 6. RSIL: This scenario considers riverine Si fluxes.

[25] 7. RF99: This scenario considers riverine Fe inputs with 99% dissolved Fe lost in estuaries.

Table 2. Mean Absolute Error (MAE) Between PISCES-T Simulations (Average 1998–2005) and Available Data for the Global Ocean

	Mean Absolute Error					
Simulation	SeaWiFS[a], mg Chla m^{-3}	NO_3[b], μM	Si[c], μM	PP – 2005[d], g C m^{-2} a^{-1}	EP – 2002[e], g C m^{-2} a^{-1}	Dissolved O_2[f], μM
NO_RIVER	0.245	2.91	11.46	53.69	12.99	10.14
RDIC	0.245	2.91	11.46	54.21	13.28	10.10
RDOC	0.203	3.20	11.44	53.65	12.98	10.34
RPOC	0.202	2.60	10.06	55.12	13.27	10.43
RNIT	0.200	4.37	11.43	57.89	13.05	10.21
RSIL	0.201	2.83	11.55	53.52	13.00	10.21
RF99	0.204	2.88	11.40	53.85	12.99	10.15
TODAY	0.197	3.25	11.44	54.52	12.98	10.51
TODAY_HiFe	0.196	3.03	10.87	56.16	13.19	10.73
HIGH_N	0.195	3.23	10.85	57.52	13.11	10.62

[a]Surface chlorophyll *a* (Chla), Seaviewing Wide Field-of-view Sensor (SeaWiFS) data.
[b]Surface NO_3 [*Conkright et al.*, 2002; *Levitus et al.*, 1994].
[c]Surface Si [*Conkright et al.*, 2002].
[d]Integrated PP from satellite data [*Behrenfeld et al.*, 2005].
[e]Export of OC below 133 m from an inversion model [*Schlitzer*, 2002].
[f]Surface dissolved O_2 [*Locarnini et al.*, 2002].

[26] 8. TODAY: This scenario is our ''best guess'' for representing today's river nutrient inputs. It considers riverine DIC, DOC, POC, DIN, Si, and low-Fe inputs. Riverine OC is considered to have the same turnover time as marine OC.

[27] 9. TODAY_HiFe: This scenario considers the same inputs of DIC, DOC, POC, DIN, and Si as in TODAY. Additionally, it has high riverine Fe input (considering 80% dissolved Fe lost in the estuaries).

[28] 10. HIGH_N: This scenario represents a future situation with higher nutrient inputs. It considers riverine DIC, DOC, POC, high DIN, Si, and high Fe (considering 80% dissolved Fe lost in estuaries). We used riverine DIN fluxes calculated for the year 2050.

[29] Except for the change in nutrient river loads, the simulations were identical.

[30] We used the average of the absolute difference between modeled parameter (a_n) and available data (c_n) values to estimate how the model simulates chlorophyll *a*, NO_3, Si, primary production, export production and dissolved O_2 (equation (2)). This also allows us to assess how riverine nutrient fluxes affect these parameters. We calculate the mean absolute error (MAE) as follows:

$$\frac{|a1 - c1| + |a2 - c2| + \ldots + |an - cn|}{n} \quad (2)$$

3. Results

3.1. Standard Simulation TODAY

[31] The scenario TODAY is our best estimate of the current input of nutrients by rivers, and of the global marine biogeochemistry. This simulation reproduces the main characteristics of ocean biogeochemistry, detailed here and in Table 2.

[32] The global surface chlorophyll *a* (Chla) generally matches the NASA's Seaviewing Wide Field-of-view Sensor (SeaWiFS) (Figures 2a and 2b and Table 2). Observed concentrations below 0.1 mg Chla m^{-3} found in the oligotrophic gyres are reproduced by the model. In the high latitudes of the Northern Hemisphere, the model estimates high concentrations (>0.4 mg Chla m^{-3} for the annual mean). However, it fails to reproduce the elevated concentrations (>2 mg Chla m^{-3} for the annual mean) observed in the shelf areas, especially in the North Atlantic (Figures 2b and 2c).

[33] The simulated gross annual primary production (PP, 95% of which is particulate, 5% as DOC) is 72.6 Pg C a^{-1} and 9.4 Pg C a^{-1} in the open and coastal ocean, respectively (Table 3 and Figure 3a). These values are higher compared to databased estimates of open ocean PP (35–67 Pg C a^{-1}) but still reasonable compared to other general circulation models coupled to biogeochemistry models (36 Pg C a^{-1} up to 78 Pg C a^{-1}) and considering the uncertainty of different estimates [*Carr et al.*, 2006]. Comparing our modeled PP to the satellite-estimated PP by *Behrenfeld and Falkowski* [1997] there is an excess in modeled PP mainly in the Southern Ocean and in the subtropical gyres. Comparing PISCES-T results to the recent satellite estimate of *Behrenfeld et al.* [2005], most of the discrepancies occur in the Southern Ocean, where the satellite-based estimates show large disagreement (Figure 3b). PISCES-T also overestimates PP (compared to *Behrenfeld et al.* [2005]) in the equatorial Atlantic Ocean. Satellite estimates of PP and Chla in this area can be biased because of the high amounts of colored dissolved organic matter discharged by large rivers (Orinoco, Amazon, Congo). The MAE between simulation TODAY and the satellite-based primary production from *Behrenfeld et al.* [2005] is low (Table 2).

[34] Our simulated export production (EP) is 9.4 Pg C a^{-1} and 0.97 Pg C a^{-1} in the open and coastal ocean, respectively. In PISCES-T, EP corresponds to the amount of particulate organic matter exported below the euphotic zone. In this version we consider it at 150 m. The global EP agrees well with observations (11 Pg C a^{-1}) [*Schlitzer*, 2002] and with results from other global carbon cycle models (8.5–15 Pg C a^{-1}) [*Aumont and Bopp*, 2006; *Schmittner et al.*, 2005]. The MAE between simulation TODAY and the data from *Schlitzer* [2002] show good agreement (Table 2). The ocean uptake of atmospheric CO_2 is −2.1 Pg C a^{-1} and −0.18 Pg C a^{-1} for the open and coastal ocean, respec-

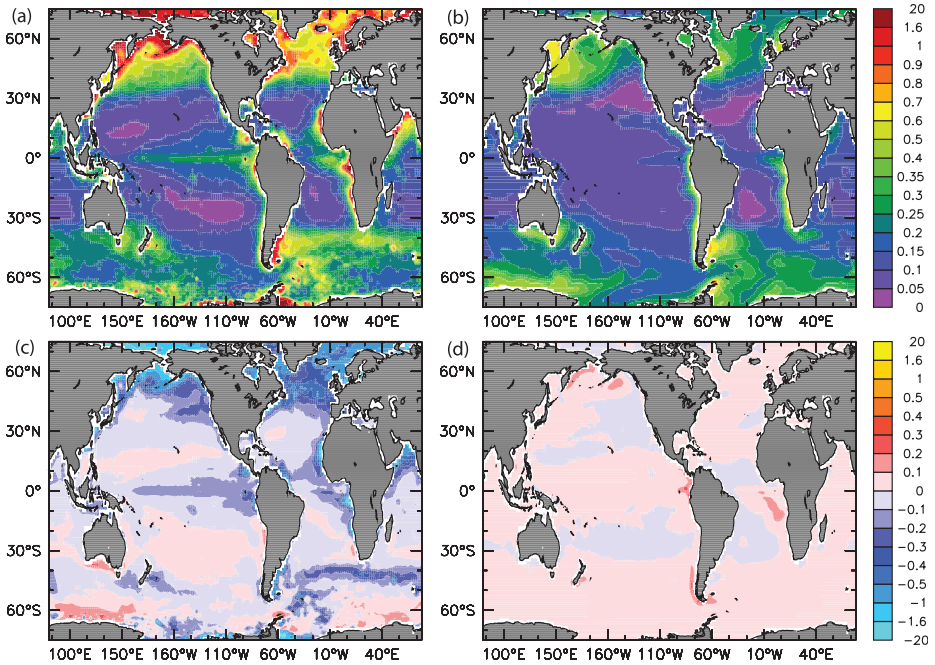

Figure 2. Annual mean surface chlorophyll *a* in mg Chla m^{-3} from (a) NASA's Seaviewing Wide Field-of-view Sensor (SeaWiFS) satellite data (average 1998–2005) and (b) standard scenario TODAY (average 1998–2005); difference in surface chlorophyll *a* (mg Chla m^{-3}) between (c) scenario TODAY and SeaWiFS and (d) the two extreme scenarios HIGH_N and NO_RIVER. Figures 2b, 2c, and 2d are an average of model results and SeaWiFS satellite data from 1998–2005.

tively. Our model results are in good agreement with the recent observation-based estimate CO_2 uptake by the coastal ocean of −0.22 Pg C a^{-1} from *Cai et al.* [2006].

[35] Our simulation reproduces the spatial surface distribution of nutrients, with the high nutrient-low chlorophyll regions observed in the equatorial Pacific, North Pacific, and Southern Ocean, low Si in the subpolar region of the Southern Ocean, and relatively high Fe concentration in the North Atlantic (Figure 2 and Table 2).

[36] Our simulation reproduces the spatial surface dissolved O_2 distribution compared to *Locarnini et al.* [2002] (Table 2). The main modeled O_2 minimum zones (dissolved O_2 concentration <25 μM) are the tropical eastern Pacific, Arabian Sea and Bay of Bengal. These areas correspond to 1.8% of the global ocean area in simulation TODAY (6.5 10^{12} m^2, Table 4). In this scenario, 35% of low-O_2 zones are located over the coastal ocean.

3.2. Impacts of Individual River Loads on Surface Chlorophyll, Nutrients, Primary Production, Export Production, Sea-to-Air CO_2 Fluxes, and Dissolved Oxygen

[37] Comparing MAE values between modeled global ocean Chla (average of years 1998–2005) and SeaWiFS data (average of years 1998–2005), the changes are not significant despite the change in river nutrient inputs (Table 2). Our results suggest that when riverine organic C, N, Si and Fe

Table 3. Primary Production (PP), Export Production (EP), and Sea-to-Air CO_2 Fluxes (CFLX) in Pg C a^{-1} for Each Scenario, Considering Global and Coastal Oceans[a]

Simulation	GLOBAL PP	COASTAL PP	GLOBAL EP	COASTAL EP	GLOBAL CFLX	COASTAL CFLX
NO_RIVER	68.7 (−5)	7.7 (−16)	9.0 (−4)	0.86 (−11)	−2.20 (+5)	−0.24 (+34)
RDIC	68.7 (−5)	7.7 (−16)	9.0 (−4)	0.86 (−11)	−2.07 (−1)	−0.20 (+16)
RDOC	70.2 (−3)	8.3 (−10)	9.1 (−3)	0.88 (−9)	−2.10 (0)	−0.20 (+16)
RPOC	75.0 (+3)	8.4 (−9)	10.1 (+8)	0.94 (−4)	−2.73 (+30)	−0.24 (+37)
RNIT	77.8 (+7)	10.5 (+14)	9.7 (+3)	1.02 (+5)	−2.79 (+33)	−0.39 (+120)
RSIL	68.6 (−6)	7.7 (−16)	9.1 (−3)	0.88 (−9)	−2.23 (+6)	−0.24 (+39)
RF99	68.9 (−5)	7.7 (−17)	9.1 (−3)	0.86 (−11)	−2.23 (+6)	−0.24 (+39)
TODAY	72.6	9.2	9.4	0.97	−2.09	−0.18
TODAY_HiFe	75.9 (+5)	9.2 (0)	10.0 (+7)	1.00 (+3)	−2.35 (+12)	−0.19 (+6)
HIGH_N	76.5 (+5)	9.6 (+5)	10.0 (+6)	1.02 (+5)	−2.49 (+19)	−0.22 (+24)

[a]The number in parenthesis corresponds to the change in percent relative to scenario TODAY. Negative values for CFLX indicate an uptake of atmospheric CO_2 by the ocean.

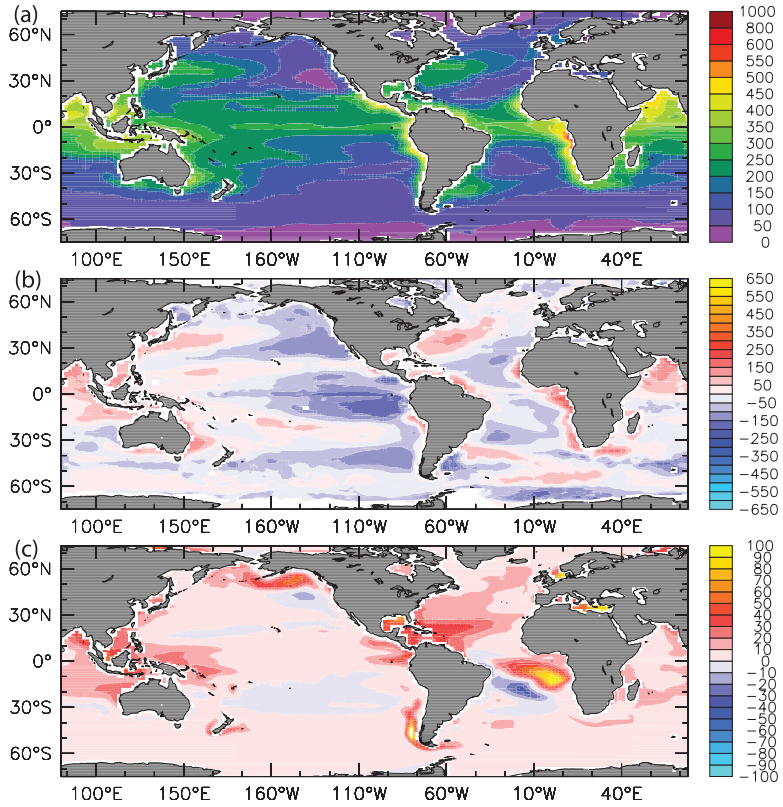

Figure 3. (a) Average (1998–2005) mean fields of integrated PP from the standard scenario TODAY in mg C m^{-2} a^{-1}; (b) difference in integrated PP in mg C m^{-2} a^{-1} between the scenario TODAY (average 1998–2005) and satellite-based PP from *Behrenfeld et al.* [2005]; and (c) difference in integrated PP between the standard scenario TODAY and the PP range of the two extreme scenarios (HIGH_N minus NO_RIVER). This is a change in percent compared to scenario TODAY ([HIGH_N-NO_RIVER] × 100/[TODAY]).

inputs are simultaneously added (TODAY, TODAY_HiFe, and HIGH_N), modeled surface Chla patterns agree better to SeaWiFS data, especially in the North Pacific, and in the Tropical Atlantic (Figure 2b). Regionally, average surface Chla concentration increases mainly in scenarios RSIL and RNIT. River Fe alone (RF99) inputs slightly increase Chla in eastern margin areas. In river-dominated areas, like the Bay of Bengal, North Brazil Shelf or Gulf of Guinea, average Chla values increase in scenarios TODAY, TODAY_HiFe, and HIGH_N (combined river nutrient inputs). In these scenarios, Chla values reach up to 10 mg Chla m^{-3} (North Brazil Shelf), comparable to SeaWiFS data. Our results suggest that in-

Table 4. Extension of Simulated Low-O_2 Areas (Average Dissolved O_2 Concentration is Below 25 μM) in the Global and Coastal Ocean

Simulation	GLOBAL OCEAN, m^2	Percent of Global Ocean Area[a]	COASTAL OCEAN, m^2	Percent of Coastal Ocean Area[b]	Percent of Global Ocean Low-O_2 Area[c]
NO_RIVER	5.50×10^{12}	1.53	1.80×10^{12}	5.60	32
RDIC	5.47×10^{12}	1.59	1.77×10^{12}	5.83	32
RDOC	5.67×10^{12}	1.59	1.86×10^{12}	6.13	33
RPOC	9.12×10^{12}	2.55	2.62×10^{12}	8.65	29
RNIT	6.57×10^{12}	1.84	2.10×10^{12}	6.94	32
RSIL	5.69×10^{12}	1.60	1.93×10^{12}	6.37	34
RF99	5.58×10^{12}	1.56	1.82×10^{12}	5.99	33
TODAY	6.54×10^{12}	1.83	2.32×10^{12}	7.65	35
TODAY_HiFe	7.69×10^{12}	2.15	2.54×10^{12}	8.40	33
HIGH_N	8.02×10^{12}	2.25	2.61×10^{12}	8.63	33

[a]Total global ocean area = 3.569×10^{14} m^2;
[b]Total coastal ocean area = 3.03×10^{13} m^2;
[c]This column shows how much (in percent) of the global ocean low-O_2 area correspond to coastal ocean.

Table 5. Modeled Coastal Ocean EP (N, Si and Fe), Riverine Inputs (N, Si, and Fe) and Ratios Between Riverine Inputs and EP[a]

Simulation	EP_N, Tmol a^{-1}	EP_Si, Tmol a^{-1}	EP_Fe, Gmol a^{-1}	Riv N, Tmol a^{-1}	Riv Si, Tmol a^{-1}	Riv Fe, Gmol a^{-1}	Riv N: EP_N, %	Riv Si: EP_Si, %	Riv Fe: EP_Fe, %
NO_RIVER	9.4	21.3	0.36	0.0	0.0	0.0	0	0	0
RDIC	9.4	21.2	0.36	0.0	0.0	0.0	0	0	0
RDOC	9.7	21.4	0.37	2.1	0.0	0.08	22	0	21
RPOC	10.2	17.9	0.39	1.6	0.0	0.06	16	0	16
RNIT	11.1	21.1	0.42	1.2	0.0	0.0	11	0	0
RSIL	9.7	24.1	0.37	0.0	6.7	0.0	0	28	0
RF99	9.4	21.4	0.36	0.0	0.0	0.32	0	0	89
TODAY	10.6	24.2	0.40	4.9	6.7	0.46	46	28	114
TODAY_HiFe	10.9	22.8	0.42	4.9	6.7	6.64	45	29	1593
HIGH_N	11.1	22.4	0.42	7.1	6.7	6.64	64	30	1567

[a]The number in parenthesis corresponds to the change in percent relative to scenario TODAY. Negative values for CFLX indicate an uptake of atmospheric CO_2 by the ocean. The number in parenthesis corresponds to the change in percent relative to scenario TODAY. Negative values for CFLX indicate an uptake of atmospheric CO_2 by the ocean. The ratio gives an estimate of the how much of the coastal EP is supported by riverine nutrients. N and Fe coastal ocean EP values were estimated using the model molar ratios of C:N (7.6:1), and C:Fe ($1:5 \times 10^{-6}$), Si coastal ocean EP is estimated by the model.

cluding river nutrients in the model improves the simulation of surface Chla. Improvements to coastal ocean representation in the model would further enhance coastal Chla simulation including increase in seasonal variability.

[38] PISCES-T simulations reproduce well surface nutrient concentrations (Table 2). In PISCES-T, NO_3 and Si surface concentrations are slightly higher when compared to World Ocean Atlas 2001 data [*Conkright et al.*, 2002]. When riverine DOC and POC are included, surface concentrations of NO_3 and Fe increase slightly on coastal areas, while surface Si decreases in the same areas. When riverine Fe is added (RF99, TODAY, TODAY_HiFe, HIGH_N), surface concentrations of NO_3 and Si decrease mainly in the tropical Atlantic and in eastern margin areas. In simulations RNIT and RSIL, our results suggest an increase in surface NO_3 and Si, respectively, in coastal areas adjacent to large river inputs.

[39] Riverine N has the highest impact on global and coastal PP. Compared to scenario TODAY, PP increases up to 7% and 14% in the global and coastal ocean, respectively. Riverine N also impacts global and coastal ocean EP (up to +3% and +5%, Table 3).

[40] Compared to scenario TODAY, river POC inputs may increase global ocean PP up to 3%, but it has a negative impact on the coastal ocean (scenario RPOC). Riverine POC alone (scenario RPOC) has the highest impact on global ocean EP. Compared to scenario TODAY, global EP increases up to 8% (Table 3). It has, however, a negative impact on coastal ocean EP. This suggests that the fast POC degradation makes nutrients available, and these are taken up by phytoplankton (mainly diatoms), which are transported to the open ocean where they are exported. This hypothesis is supported by slightly lower modeled coastal ocean diatom biomass in scenario RPOC (1.0 Pg C a^{-1}, average of 1998–2005) compared to NO_RIVER (1.1 Pg C a^{-1}, average of 1998–2005), and by the low modeled Si export in the coastal ocean in scenario RPOC (17.9 Tmol Si a^{-1}, average of 1998–2005, Table 5) compared to NO_RIVER (21.3 Tmol Si a^{-1}, average of 1998–2005, Table 5).

[41] Riverine DIC, Si, or Fe, when added alone, have very little impact on PP and EP (Table 3). Riverine DOC brings additional N and Fe, thus increasing global and coastal PP. Its impact on EP is low compared to scenario NO_RIVER because Si may become a limiting nutrient for diatoms. Riverine DOC is also less labile than riverine POC, which also contributes to its lower impact on PP and EP. Riverine Fe has a fertilizing effect on the global ocean when it is combined to N and Si inputs. In scenario TODAY_HiFe our results suggest that more available riverine Fe (N, Si and C remain unchanged compared to scenario TODAY) impacts the open ocean PP and EP, with little changes in the coastal ocean (Table 3). Increasing riverine Fe together with riverine N (scenario HIGH_N) impact the coastal ocean primary and export production (Table 3).

[42] Riverine N has the highest impact on sea-to-air CO_2 flux (Table 3). In the global ocean, the CO_2 sink increases up to 0.59 Pg C a^{-1} compared to scenario NO_RIVER, and up to 0.15 Pg C a^{-1} in the coastal ocean. In both areas the sink increase is equivalent to the increase in export production. Riverine DIC and DOC inputs decrease the ocean CO_2 sink. In these cases part of the dissolved carbon is outgassed to the atmosphere.

[43] Low-O_2 areas extension varies little when individual nutrients are added, except in scenarios RPOC, and RNIT to a lesser extent (Table 4). Compared to scenario TODAY, riverine POC alone may increase low-O_2 areas up to 39% and 13% in the global and coastal ocean, respectively. This result is consistent with the high impact of riverine POC on primary and export production.

3.3. Maximum Impact of River Nutrient Load

[44] The maximum impact of river nutrient load can be assessed by subtracting the zero input scenario NO_RIVER from the high river nutrient input HIGH_N. This comparison allows us to bracket the impact of nutrient loading and to identify the spatial features in global ocean biogeochemistry that are caused by river nutrient fluxes.

[45] Surface Chla concentration in HIGH_N increases (compared to NO_RIVER) regionally by up to 10 mg m^{-3} in coastal areas under large river influence, like the North Brazil Shelf, the Gulf of Guinea and the Bay of Bengal. Average surface Chla also increases in coastal eastern margin areas like the Gulf of Alaska, southeastern and tropical eastern Pacific (Figure 2d).

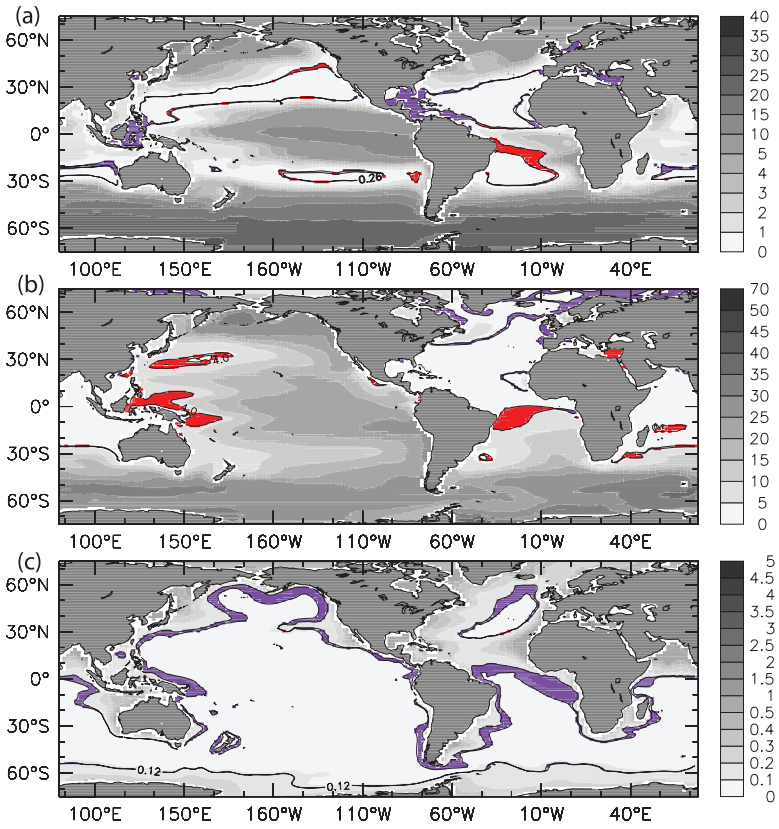

Figure 4. Average (1998–2005) surface mean fields from the standard scenario TODAY for (a) NO_3 in μM, (b) Si in μM, and (c) Fe in nM. Shaded red areas correspond to regions where surface nutrient concentration in the scenario of higher river inputs (HIGH_N) drops below the threshold contour of diatoms K_m (half saturation constant) when compared to scenario NO_RIVER. Shaded purple areas show the reverse. Thresholds are set to (Figure 4a) 0.5 μM NO_3, (Figure 4b) 4 μM Si, and (Figure 4c) 0.12 nM Fe. Purple areas give a rough indication of places where diatom nutrient limitation has been alleviated. Red shading corresponds to areas where diatom nutrient limitation has become more severe.

[46] Surface nutrient concentration is mainly affected by riverine Fe input. When Fe is added (scenarios RF99, TODAY, and TODAY_HiFe), our results show a decrease in surface NO_3 and Si, due to a relaxation of Fe limitation. Increased Fe availability in scenarios TODAY_HiFe and HIGH_N increases this effect despite the increased availability of N in the latter. Figure 4 shows the changes in diatom nutrient limitation of NO_3, Si and Fe from the NO_RIVER to the HIGH_N scenario. The red areas show where diatoms have become nutrient limited (surface concentration above the half saturation constant (K_m) in NO_RIVER and below the K_m in HIGH_N) and the purple areas show where diatom limitation for that nutrient has been alleviated. Diatom limitation of NO_3 and Si has increased mainly in the Atlantic Ocean and in the subtropical gyres, while it has been alleviated in the areas adjacent to large river inputs (Figures 4a and 4b). In contrast to NO_3 and Si, there are only areas in which surface Fe limitation has been alleviated in scenario HIGH_N compared to NO_RIVER (Figure 4c).

[47] Primary production increases by 7.8 Pg C a^{-1} (+11%, compared to NO_RIVER) in the open ocean, and by 1.9 Pg C a^{-1} (+25%, compared to NO_RIVER) in the coastal ocean (Table 3). The maximum increase in PP occurs in the areas where surface Chla increases and where river inputs are large (Figure 3c). Simulated EP is enhanced in the same regions where surface Chla and primary production increase (Figures 2d and 3c). It increases by 0.9 Pg C a^{-1} (+10% compared to NO_RIVER) in the open ocean, and 0.16 Pg C a^{-1} (+19%, compared to NO_RIVER) in the coastal ocean (Table 3). Sea-to-air CO_2 flux change is modest. In the coastal ocean, the fluxes are basically not altered (−0.02 Pg C a^{-1}), despite the increased availability of Fe (TODAY_HiFe) and N and Fe in scenario HIGH_N. In the open ocean, increased availability of N and Fe enhances production (and the biological pump), leading to an increase in CO_2 uptake (+0.29 Pg C a^{-1}) (Table 3).

[48] Enhanced EP increases the extent of modeled low-oxygen areas. In scenario HIGH_N the extent of global low-O_2 areas increases 47% compared to NO_RIVER. In the coastal ocean, the low-O_2 areas increase at the same rate (+48%, Table 4). Increased river inputs impact the same low-O_2 areas as in scenarios NO_RIVER and TODAY

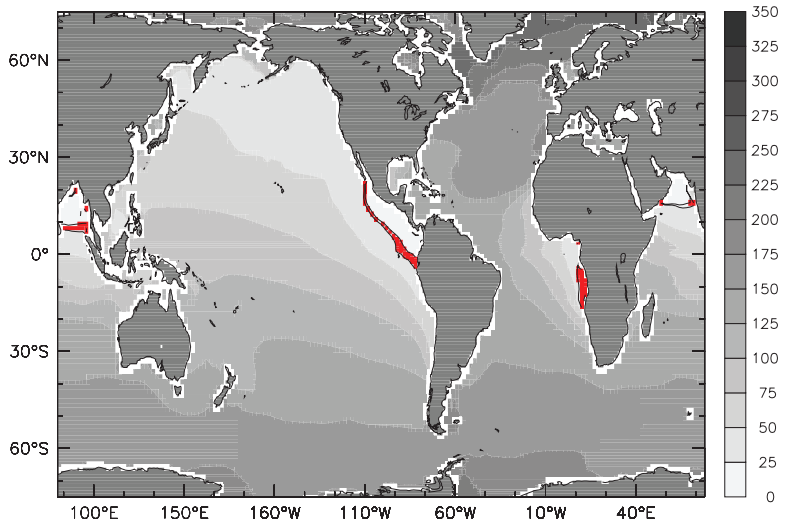

Figure 5. Annual average (1998–2005) mean fields of the minimum dissolved O_2 (in μM) in the water column from the standard simulation TODAY. Shaded red areas correspond to regions where the low dissolved O_2 (dissolved $O_2 < 25$ μM) concentration in the scenario of high river inputs (HIGH_N) extend beyond the threshold contour (25 μM) of the scenario without river inputs (NO_RIVER).

along with the area adjacent to the Congo river outflow off western African coast (Figure 5).

4. Discussion

4.1. Impacts of River Loads on Primary Production

[49] River nutrients have a modest impact on the biogeochemistry of the global and coastal oceans (Table 3). Considering scenario TODAY as standard, our results suggest that global ocean PP would decrease up to −5% if riverine nutrients were to cease completely (NO_RIVER), while it would increase up to +5% if we consider that nutrient delivery increase with increasing population (HIGH_N). The modest effect of riverine nutrient loading on PP may be affected by too low a sensitivity to added nutrient loads. The excess in our modeled PP compared to satellite-estimated PP by *Behrenfeld et al.* [2005] in the subtropical gyres and coastal areas suggests that nutrient availability in the upper ocean is higher in the model, leaving less scope for increases by river supply.

[50] The influence of increasing just one nutrient can be limited, because it simply decreases the availability of the other nutrients. On the one hand, simulated variation of riverine Fe inputs from 0.0 (NO_RIVER) to 0.32 Gmol Fe a^{-1} (RF99) suggests that there are no changes in open and coastal oceans primary production. In scenario RF99, surface NO_3 and Si concentrations decrease, mainly in eastern margin areas. Simulated variation of riverine Si from 0.0 (NO_RIVER) to 6.7 Tmol Si a^{-1} do not change either the open or coastal oceans primary production. Besides, atmospheric deposition (Fe and Si) and resuspension (Fe) act as additional sources of these nutrients to the oceans. Atmospheric inputs remain the main source of Fe and Si in open ocean areas like the subtropical eastern Atlantic (Sahara dust inputs). On the other hand, simulated variation of riverine N inputs from 0.0 (NO_RIVER) to 1.2 Tmol N a^{-1} (RNIT) suggests that open ocean primary production may increase up to 9.1 Pg C a^{-1} in the open ocean and 2.8 Pg C a^{-1} in the coastal ocean. This suggests that riverine N may have the higher impact in coastal and open ocean biological carbon pump. Our simulated export production and sea-to-air CO_2 results corroborate this statement.

[51] In scenarios RDOC and RPOC, organic carbon is also a source of N and Fe. The amounts of riverine N in these simulations are comparable to scenario RNIT. River POC has a higher impact on open ocean primary and export production. Although the amount of riverine OC input is smaller (and thus riverine N and Fe) in RPOC, faster particulate OC degradation could explain the higher impact in PP. Thus riverine POC faster degradation acts as a source of nutrients, which are taken up by diatoms. These are further transported off the coastal ocean, and leading to an increase in EP and in the ocean CO_2 sink (Table 3).

[52] In scenarios considering riverine Fe (RDOC, RPOC, RF99, TODAY, TODAY_HiFe, HIGH_N), combined or not to other nutrients, PP and EP are enhanced in areas where upwelling and high runoff are combined, mainly in eastern margins. The increased availability of dissolved Fe combined with N and Si has a fertilizing effect for the timescale considered in this study. As a consequence of enhancing PP in the coastal ocean, N and Si are more consumed and depleted in the surface (Figures 4a and 4b). The lateral export of N and Si to the open ocean is reduced because of a more efficient export of organic matter to deeper layers, and surface nutrient concentrations in TODAY, TODAY_HiFe, and HIGH_N are lower than in scenario NO_RIVER. Our results suggest this effect is accentuated in the tropical Atlantic area, where the South Equatorial Current transports nitrate-impoverished surface water westward to the NE Brazilian coast, where it splits northwestward and south-

ward. In this zone the river inputs are reduced and thus nutrient limitation decreases primary production up to 30% in the coast and adjacent subtropical gyre (Figure 3c). Over longer timescales (centuries) increased availability of Fe may lead to a reduction in primary production due to N and Si depletion. In our simulations, regions like the N-Brazil Shelf had slightly reduced primary and export production when only riverine Fe is added (RF99 minus NO_RIVER), or when riverine Fe input increases alone (TODAY_HiFe minus TODAY). Our findings are consistent with those of *Aumont et al.* [2003], who ran 500-a simulations considering an increase in Fe atmospheric inputs.

4.2. Nutrient Limitation: How Much of Coastal Ocean Production is Sustained by Riverine Nutrients?

[53] The coastal zone is more sensitive to riverine loads of nutrients. Compared to scenario TODAY, the coastal PP would decrease up to −16% in scenario NO_RIVER, while it would increase up to +5% in scenario HIGH_N. Our results suggest that the PP in the coastal ocean is mainly limited by N and Si inputs. The modeled coastal ocean and subtropical gyres are mainly limited by N or Si (in case of diatoms), and some eastern margin zones are Fe-limited (see Figure S1).[1] It explains why riverine N alone has the highest impact on coastal ocean production, and why riverine Fe has a higher impact in the eastern margin areas, despite the relatively small local runoff (Figure 1).

[54] When Fe is added to the oceans, the coastal area becomes increasingly N- and/or Si-limited. The Atlantic Ocean is more affected by Si limitation, especially over continental margins and in the tropical areas adjacent to large river outflow (Amazon and Orinoco on the western side, Congo and Niger on the eastern side). Our results suggest that the limited impact of river inputs in global and coastal ocean production is partly explained by the increase in N and Si limitation in surface waters, especially when larger amounts of river Fe enter the ocean (scenarios TODAY_HiFe and HIGH_N). The excess Fe is exported to open ocean areas. This is corroborated by the simultaneous impoverishment in N and Si concentrations in surface waters and enrichment in surface Fe (Figure 4). Excess nutrients in coastal areas increase the primary production locally if the conditions of nutrient limitation are favorable. However, it may deplete nutrients in surface waters in the central ocean gyres because of a higher vertical export of organic matter before the water masses reach these areas, as in the Pacific Ocean.

[55] We calculated nutrient budgets (N, Si and Fe) for the coastal ocean using the ratio between modeled riverine inputs and EP (Table 5). This gives a first-order estimate of the proportion of the EP supported by riverine nutrients in the coastal ocean. The corresponding N and Fe coastal export production was estimated using the model molar ratios of C:N (122:16) and C:Fe ($122{:}6.1 \times 10^{-4}$), and Si coastal export production is calculated by PISCES-T.

[56] In all scenarios RDOC, RPOC, RNIT, TODAY, and TODAY_HiFe, riverine N inputs may sustain up to 46% of the coastal EP. Increasing N flux (HIGH_N) reduces the coastal N limitation, and future riverine N fluxes would sustain up to 64% of coastal EP. In scenarios RSIL, TODAY, TODAY_HiFe, and HIGH_N, riverine Si fluxes would sustain up to 30% of coastal EP, with large regional variations. In scenario HIGH_N, riverine fluxes of Fe would fully sustain the coastal EP therefore we estimate the highest enhancement in coastal production. Regional response to riverine N and Si may be very variable which denotes differences in regional nutrient limitation. On the one hand, western margins influenced by high river runoff are N-limited at different levels. In these areas, riverine Si and Fe are able to sustain EP. On the other hand, in eastern margins dominated by upwelling, river inputs of N and Si do not sustain EP. In these areas, only Fe export production is sustained by riverine inputs in scenarios RF99, TODAY, TODAY_HiFe, and HIGH_N, despite regional variation in riverine input (Figure 1).

[57] Accordingly, our results suggest that most of the EP in the coastal ocean may be sustained by nutrient transport from the open ocean, by local nutrient recycling, and by sediment resuspension. This has been previously suggested by *Wollast* [1998] and *Ducklow and McCallister* [2004].

4.3. Consequences for Ecosystem Structure

[58] Changes in nutrient ratio delivery to the coastal ocean may have consequences for the ecosystem structure. Until recently, there has been only speculation about the potential effects of decreased riverine Si inputs [*Conley et al.*, 1993; *Humborg et al.*, 2000] and changes in other nutrient inputs [*Jickells*, 1998] on coastal ecosystems.

[59] Total phytoplankton PP is highly influenced by N, Fe, and Si riverine inputs, in this order. Diatom primary production in the coastal zone is increased by Fe (and presumably Si), and decreased by N. Our results suggest that their biomass would decrease up to −9% if riverine fluxes were stopped (NO_RIVER), and increase up to 13% in scenario TODAY_HiFe, and 5% in scenario HIGH_N, compared to TODAY. Si is a limiting nutrient for diatoms mainly in the coastal ocean, North Atlantic and some areas of the Southern Ocean. The Si-limited zones extend over eastern margin areas, especially in the equatorial eastern Atlantic in scenarios where Fe is added (Figure 4 and Figure S1).

[60] Nanophytoplankton production is less influenced by riverine inputs. Globally, if riverine nutrient fluxes were to stop (NO_RIVER), nanophytoplankton biomass would decrease up to −3% compared to TODAY. Its biomass would increase up to 3% in HIGH_N. In our model, nanophytoplankton is Fe-limited everywhere, except in some coastal areas and in tropical North Atlantic. Riverine Fe availability enhances N limitation for nanophytoplankton in the coastal and open ocean areas under the influence of large river plumes like in the tropical Atlantic.

[61] There is no shift in phytoplankton composition when river nutrients are added to the model. In all scenarios the total phytoplankton biomass proportions remain unchanged, i.e., 66–67% of nanophytoplankton and 34–33% of diatoms.

[62] The changes in phytoplankton production impact the zooplankton biomass. Open ocean microzooplankton response to riverine nutrients is modest, ranging from −7% (NO_RIVER) to +4% (HIGH_N) of its biomass. Mesozooplankton biomass instead responds noticeably to variations

[1] Auxiliary materials are available in the HTML. doi:10.1029/2006GB002718.

in diatom production (TODAY_HiFe and HIGH_N) and to a lesser extent to the increased availability of riverine small POC. We estimate globally a variation range from −7% (NO_RIVER) to +13% (TODAY_HiFe) and +6% (HIGH_N) in mesozooplankton biomass. Mesozooplankton contribution to vertical particle flux, thus export production, is larger than that of microzooplankton. Because they are also an important source of food for fishes, alterations in ecosystem structure because of nutrient availability could lead to changes in fisheries yields.

4.4. Consequences for Carbon Export and CO_2 Fluxes

[63] River nutrient fluxes impact PP and ecosystem composition, both of which play a major role for EP and CO_2 fluxes. We estimate modest changes in EP. We estimate a decrease up to 0.3 PgC a^{-1} (−4%) in scenario NO_RIVER in open ocean export production, and an increase up to 0.6 Pg C a^{-1} (+6%) in scenario HIGH_N.

[64] About 75% of the changes in EP are subsequently drawn from the atmosphere (the other 25% are probably drawn from ocean DIC), except for the scenarios where river IC and OC are considered (see section 4.5). We estimate an increase in the open ocean CO_2 sink up to +0.11 Pg C a^{-1} (+5%) in scenario NO_RIVER, and an increase up to +0.4 Pg C a^{-1} (+19%) in scenario HIGH_N. *Matear and Elliott* [2004] used this concept of "carbon sequestration efficiency" to evaluate the impacts of macronutrient fertilization scenarios in a global ocean carbon model. In their P-fertilization scenario they found that decreasing P-limited areas increased the ocean CO_2 sink. Our model scenarios show the same response considering an increase in riverine N fluxes to the ocean. The effect of riverine N on the ocean CO_2 sink is stronger in the coastal area, although the amount of carbon is small. This suggests that the increase in PP by riverine inputs is counter-balanced by an increase in organic matter respiration owing to increased transport of terrestrial OC and increased organic matter from new production. Our results are in agreement with the model findings of *Mackenzie et al.* [2004].

4.5. What Happens to River OC Inputs?

[65] We estimate that up to 110 Tg C a^{-1} of river OC are rapidly mineralized and returned to the atmosphere (global CO_2 flux TODAY – NO_RIVER). This corresponds to 25% of the amount of delivered river OC. On a simple calculation using model results we have river POC = 147.6 Tg C a^{-1}, difference in coastal export production (ΔPOC, scenarios RPOC – NO_RIVER) = 80 Tg C a^{-1}, difference in coastal sea-to-air CO_2 flux (ΔCO_2, scenarios RPOC – NO_RIVER) = 0 Tg C a^{-1}, and river POC – (ΔPOC + ΔCO_2) = 147.6 − 80 = 67.6 Tg C a^{-1}. This difference corresponds to the amount of river POC exported to the open ocean area. The model resolution does not allow the typical water entrapment of coastal areas (and thus particles), leading to a larger export of riverine POC (46%). Literature databased values estimate that up to 80% of the riverine POC is trapped in the coastal area, being mineralized or buried in the sediments [*Muller-Karger et al.*, 2005].

[66] Riverine DOC is mineralized, and part of this carbon returns to the atmosphere. Repeating the same calculation above we have river DOC = 189.6 Tg C a^{-1}, difference in export production (ΔDOC, scenarios RDOC – NO_RIVER) = 20 Tg C a^{-1}, difference in sea-to-air CO_2 flux (ΔCO_2, scenarios RDOC – NO_RIVER) = 40 Tg C a^{-1}, and river DOC – (ΔDOC + ΔCO_2) = 189.6 − 60 = 129.6 Tg C a^{-1}. This difference corresponds to the amount of river DOC exported to the open ocean area. Further river DOC mineralization and export happen in the open ocean: 60 Tg C a^{-1} are outgassed, and 70 Tg C a^{-1} remain in the open ocean.

[67] Riverine DIC is also outgassed to the atmosphere. Our results suggest that up to 130 Tg C a^{-1} is returned to the atmosphere (ΔCO_2, scenarios RDIC – NO_RIVER, Table 3).

[68] The differences between river carbon fate in scenarios RPOC and RDOC are mainly due to the behavior of small POC and DOC in PISCES-T. Small POC degradation is 10 times faster than DOC at 0°C and at the ocean surface. Additionally, POC degradation increases with temperature while DOC degradation decreases with depth. Thus additional N and Fe in scenario RPOC are more rapidly available to phytoplankton compared to scenario RDOC, despite the amount of nutrient inputs being smaller. On the one hand, coastal PP in scenarios RPOC and RDOC are very similar (Table 3). On the other hand, coastal EP is 51 Tg C a^{-1} larger in scenario RPOC than in scenario RDOC (Table 3). This increase in EP is then reflected in a coastal air-sea CO_2 flux (CFLX) that is 41 Tg C a^{-1} larger in scenario RPOC than in scenario RDOC, which corresponds to 80% of the difference in EP above. Additional evidence that in scenario RPOC nutrients are more rapidly available is the larger increase in phyto- and zooplankton biomass relative to scenario NO_RIVER. In RPOC, diatoms biomass increases up to 9% compared to NO_RIVER, with no change in scenario RDOC. Microzooplankton biomass also increases more in scenario RPOC (up to +19%) than in scenario RDOC (up to +3%) relative to NO_RIVER.

[69] In scenario TODAY, sea-to-air fluxes are similar to RDIC and RDOC. Further addition of N and Fe (TODAY_HiFE and High_N) does not change much of coastal ocean CO_2 fluxes, while open ocean sea-to-air CO_2 fluxes may increase up to 0.4 PgC a^{-1}. This suggests that additional nutrient inputs are insufficient to decrease the mineralization of dissolved organic matter mainly in the coastal ocean, as predicted by *Ludwig et al.* [1996b] and *Smith and Hollibaugh* [1993]. Our findings may be used as a baseline for scenarios considering the impact (uptake/degassing) of anthropogenic CO_2. In this study, we considered the same reactivity for terrestrial and marine OC. On the one hand, field studies showed that terrestrial OC may have slower degradation rates than marine OC, not being immediately available as a source of nutrients to plankton [*Dittmar and Kattner*, 2003; *Hansell et al.*, 2004]. On the other hand, in densely populated basins, riverine OC may have a high-anthropogenic fraction that is more labile [*Harrison et al.*, 2005]. Regional differences in riverine OC reactivity and photodegradation rates may change the availability of nutrients for biological uptake [*Del Vecchio and Subramaniam*, 2004].

4.6. Oxygen Minimum Zones

[70] Our model simulations show that PP and EP are enhanced in areas where upwelling and high runoff are

combined, mainly in eastern margins. This production material sinks and is decomposed in midwater, consuming dissolved O_2. When high O_2 demand occurs in combination with slower circulation and O_2-poor waters, significant midwater O_2 minima develop [*Helly and Levin*, 2004]. Low-O_2 (where dissolved $O_2 < 25$ μM) zones are found in large areas of the eastern Tropical Pacific, Arabian Sea, Bay of Bengal, and the tropical eastern Atlantic, in agreement with typical low-O_2 areas previously described by *Helly and Levin* [2004] and *Reichart et al.* [1998]. In our simulations, the coastal low-O_2 areas extend from 1.8×10^{12} m^2 (NO_RIVER) to 2.6×10^{12} m^2 (+45%, HIGH_N) (Table 4 and Figure 5). Riverine POC alone (scenario RPOC) is responsible for the highest increase in global ocean low-O_2 areas (9.12×10^{12}, +66% compared to NO_RIVER). The enhanced sinking of particulate organic matter (enhanced diatom and fecal pellet production in scenario RPOC) adds to the decomposition of marine particles and thus to O_2 consumption in the water column.

[71] Our results suggest that riverine Fe fluxes have a strong influence on the extent of the low-O_2 areas, especially on the Gulf of Guinea. This area is characterized by high river runoff from three large river systems: the Volta and Niger rivers at its north portion, and the Congo river at the southernmost area [*Ukwe et al.*, 2003]. The extent and severity of low-O_2 areas affect the marine trophic chain because benthic marine life may be severely disturbed. Losses in biological diversity or decline in primary production may lead to deleterious impacts on local fisheries resources. Finally, larger extents of low-O_2 areas in the oceans may alter microbial respiration thus leading to a change in sea-air fluxes of the greenhouse gases N_2O and CH_4.

4.7. Regional Impacts

[72] River inputs of nutrients and OC are unevenly distributed. The ratio of delivered riverine nutrients and OC combined with the local nutrient budget and adjacent ocean dynamics are factors controlling the regional impacts. In the Gulf of Guinea, southeastern Pacific, and northeastern Pacific, riverine nutrients do not sustain much of the local EP but strongly enhance PP. Our results suggest that a nutrient trapping effect is caused by slower circulation in these areas, thus having a fertilizing effect. Increased Fe availability results in excess Fe in the eastern Tropical Atlantic. The excess Fe from the Gulf of Guinea rivers is exported to the open ocean, increasing PP in an extended area (Figure 3c). In other nonupwelling areas adjacent to large river outflow (Amazon, Mississippi, Ganges-Brahmaputra, Pearl) the increase in PP is restricted to the area adjacent to the river outflow (Figure 3c).

4.8. Limitations of the Model

[73] We present a first approach to estimate the impacts of river nutrients on the global ocean. This modeling approach can be used as a tool to assess the nutrient and carbon exchange between the coastal and the open ocean. However, our approach has limitations. First, our model does not have a real representation of the coastal zone. Because of its coarse resolution, the model is not able to resolve coastal circulation patterns, like upwelling or increased vertical mixing. A higher resolution of the coastal ocean would improve the representation of very productive zones and allow model simulations to assess its response to climate changes and increase in atmospheric CO_2. Second, we used annual mean fluxes of riverine nutrients to the ocean. In areas adjacent to strong river input like the Amazon, Orinoco or Congo, flood and drought periods alter the amount of river nutrient fluxes. Third, we use an average concentration for river Fe and Si. Development of databases considering river basin geology may alter the distribution of riverine Fe and Si significantly. Fourth, our scenarios do not consider any reduction of freshwater inputs. A reduction in the freshwater input to the coastal zone would reduce river nutrient inputs and diminish the river plume buoyancy effect on the shelves (i.e., estuarine water over seawater), which in turn reduces cross-shelf upwelling and the consequent upward nutrient input from subsurface waters and deep sea. This flow of subsurface water is, in some cases, one of the major sources of nutrients to the shelf. Subsequently, productivity and the CO_2 sink could be further diminished [*Chen et al.*, 2003]. Fifth, our model has a limited representation of the ecosystem. Including a more complex representation of the ecosystem will allow us to assess the impacts of changes on nutrient availability on plankton types and on fisheries at the regional to global scale [*Le Quéré et al.*, 2005]. Sixth, our model does not differentiate terrestrial and marine organic carbon reactivity (degradation and mineralization rates, C:N ratio). If riverine OC is more labile than marine OC, the RPOC simulation shows that a bigger impact could be expected with a transfer of productivity from the coastal to the open ocean and a bigger air-sea CO_2 sink.

[74] All these factors can enhance or dampen locally the impact of river inputs in ways that are difficult to assess, especially since our analysis of individual components did not show up as cumulative effects in the TODAY scenario. In spite of these limitations, our analysis provides a best estimate of the upper and lower bounds of the potential impact of nutrient supply by rivers considering the most up-to-date tools and data available.

5. Conclusion

[75] We assessed the potential impact of riverine nutrient inputs on ocean biogeochemistry using an ecosystem-based ocean biogeochemistry model. Our best estimate scenario for current riverine nutrient input reproduces the main characteristics of the ocean biogeochemistry.

[76] The maximum impact of river nutrients can be estimated by comparing two extreme scenarios, one where river nutrients are enhanced compared to today's values (HIGH_N), and one where river inputs are set to zero (NO_RIVER). Open ocean PP increases by 7.8 Pg C a^{-1} and coastal ocean PP by 1.9 Pg C a^{-1}. River nutrients impact mainly eastern margin areas where upwelling and high runoff are combined. The limited impact of rivers on ocean PP is explained partly by severe N and Si limitation in surface waters provoked by enhanced Fe availability.

[77] Riverine N has the larger impact on coastal oceans, followed by riverine POC and DOC. Riverine OC acts as an

important additional nutrient source, impacting both coastal and open ocean production. When combined to riverine N and Si, riverine Fe has a larger impact on the open ocean. Changes in river nutrient fluxes have a direct but small impact on the sea-air CO_2 fluxes.

[78] Increasing river nutrient inputs enlarges the low-O_2 areas under riverine influence at the eastern Tropical Pacific, Bay of Bengal, and especially in the coastal eastern tropical Atlantic under the influence of the Congo river up to +45% (scenario HIGH_N – NO_RIVER). Fluctuations in the extent of the low-O_2 areas can have significant climatic, ecological and economic impacts.

[79] Considering riverine nutrient and carbon fluxes in ocean modeling is an important step to understand their impacts and identify the associated spatial features in ocean biogeochemistry. Additionally, it can help assessing how anthropogenic changes in riverine inputs may impact the different biogeochemical provinces of the world ocean.

[80] **Acknowledgments.** We thank Petra Döll for providing the DDM30 file (GlobalNews project), NASA/GSFC/DAAC for providing SeaWiFS chlorophyll data and satellite-based ocean PP data, DKRZ for their support for the use of the NEC-SX6 computer, K. Rodgers and C. Enright for providing the forcing files, and the two anonymous reviewers for their insightful comments. L. C. da Cunha was funded by EU contract HPMD-CT-2000-00038. This study is part of the Dynamic Green Ocean Project (available at http://lgmacweb.env.uea.ac.uk/green_ocean/index.shtml).

References

Aumont, O., and L. Bopp (2006), Globalizing results from ocean in situ iron fertilization studies, *Global Biogeochem. Cycles*, *20*, GB2017, doi:10.1029/2005GB002591.

Aumont, O., J. C. Orr, P. Monfray, W. Ludwig, P. Amiotte-Suchet, and J.-L. Probst (2001), Riverine-driven interhemispheric transport of carbon, *Global Biogeochem. Cycles*, *15*(2), 393–405.

Aumont, O., S. Belviso, and P. Monfray (2002), Dimethylsulfoniopropionate (DMSP) and dimethylsulfide (DMS) sea surface distributions simulated from a global three-dimensional ocean carbon cycle model, *J. Geophys. Res.*, *107*(C4), 3029, doi:10.1029/1999JC000111.

Aumont, O., E. Maier-Reimer, S. Blain, and P. Monfray (2003), An ecosystem model of the global ocean including Fe, Si, P co-limitations, *Global Biogeochem. Cycles*, *17*(2), 1060, doi:10.1029/2001GB001745.

Behrenfeld, M. J., and P. G. Falkowski (1997), Photosynthetic rates derived from satellite-based chlorophyll concentration, *Limnol. Oceanogr.*, *42*, 1–20.

Behrenfeld, M. J., E. Boss, D. A. Siegel, and D. M. Shea (2005), Carbon-based ocean productivity and phytoplankton physiology from space, *Global Biogeochem. Cycles*, *19*, GB1006, doi:10.1029/2004GB002299.

Beusen, A. H. W., A. L. M. Dekkers, A. F. Bouwman, W. Ludwig, and J. Harrison (2005), Estimation of global river transport of sediments and associated particulate C, N, and P, *Global Biogeochem. Cycles*, *19*, GB4S05, doi:10.1029/2005GB002453.

Blanke, B., and P. Delecluse (1993), Low frequency variability of the tropical Atlantic Ocean simulated by a general circulation model with mixed layer physics, *J. Phys. Oceanogr.*, *23*, 1363–1388.

Bopp, L., K. E. Kohfeld, C. Le Quéré, and O. Aumont (2003), Dust impact on marine biota and atmospheric CO_2 during glacial periods, *Paleoceanography*, *18*(2), 1046, doi:10.1029/2002PA000810.

Boyle, E. A., et al. (1977), Mechanism of iron removal in estuaries, *Geochim. Cosmochim. Acta*, *41*(9), 1313–1324.

Buitenhuis, E., C. Le Quéré, O. Aumont, G. Beaugrand, A. Bunker, A. Hirst, T. Ikeda, T. O'Brien, S. Piontkovski, and D. Straile (2006), Biogeochemical fluxes through mesozooplankton, *Global Biogeochem. Cycles*, *20*, GB2003, doi:10.1029/2005GB002511.

Cai, W.-J., M. Dai, and Y. Wang (2006), Air-sea exchange of carbon dioxide in ocean margins: A province-based synthesis, *Geophys. Res. Lett.*, *33*, L12603, doi:10.1029/2006GL026219.

Carr, M.-E., et al. (2006), A comparison of global estimates of marine primary production from ocean color, *Deep Sea Res., Part II*, *53*(5–7), 741–770.

Chen, C. T. A., et al. (2003), Continental margin exchanges, in *Ocean Biogeochemistry*, edited by M. J. R. Fasham, pp. 53–97, Springer-Verlag, Heidelberg.

Chester, R. (1990), *Mar. Geochem.*, 698 pp., Unwin Hyman, London.

Conkright, M. E., et al. (2002), *World Ocean Atlas 2001*, vol. 4, *Nutrients*, in *NOAA Atlas NESDIS 52*, edited by S. Levitus, 392 pp., U.S. Gov. Print. Off., Washington, D. C.

Conley, D. J., et al. (1993), Modification of the biogeochemical cycle of silica with eutrophication, *Mar. Ecol. Progr. Ser.*, *101*(1–2), 179–192.

Dai, M., and J. M. Martin (1995), First data on trace metal level and behaviour in two major Arctic river-estuarine systems (Ob and Yenisey) and in the adjacent Kara Sea, *Earth Planet. Sci. Lett.*, *131*, 127–141.

de Baar, H. J. W., and J. T. M. De Jong (2001), Distributions, sources and sinks of iron in seawater, in *The Biogeochemistry of Iron in Seawater*, edited by D. R. Turner and K. A. Hunter, pp. 123–253, John Wiley, Chichester, UK.

Del Vecchio, R., and A. Subramaniam (2004), Influence of the Amazon River on the surface optical properties of the western tropical North Atlantic Ocean, *J. Geophys. Res.*, *109*, C11001, doi:10.1029/2004JC002503.

Dittmar, T., and G. Kattner (2003), Recalcitrant dissolved organic matter in the ocean: Major contribution of small amphiphilics, *Mar. Chem.*, *82*, 115–123.

Doell, P., and B. Lehner (2002), Validation of a new global 30-min drainage direction map, *J. Hydrol.*, *258*(1–4), 214–231.

Ducklow, H. W., and S. L. McCallister (2004), The biogeochemistry of carbon dioxide in the coastal oceans, in *The Sea*, vol. 13, *The Global Coastal Ocean: Multiscale Interdisciplinary Processes*, edited by A. R. Robinson and K. Brink, pp. 269–316, Harvard Univ. Press, Boston.

Dumont, E., J. A. Harrison, C. Kroeze, E. J. Bakker, and S. P. Seitzinger (2005), Global distribution and sources of dissolved inorganic nitrogen export to the coastal zone: Results from a spatially explicit, global model, *Global Biogeochem. Cycles*, *19*, GB4S02, doi:10.1029/2005GB002488.

Gaspar, P., Y. Grégoris, and J.-M. Lefevre (1990), A simple eddy kinetic energy model for simulations of the ocean vertical mixing: Tests at station Papa and long-term upper ocean study site, *J. Geophys. Res.*, *95*(C9), 16,179–16,193.

Gent, P. R., and J. C. McWilliams (1990), Isopycnal mixing in the ocean circulation models, *J. Phys. Oceanogr.*, *20*, 150–155.

Green, P., et al. (2004), Pre-industrial and contemporary fluxes of nitrogen through rivers: A global assessment based on typology, *Biogeochemistry*, *68*(1), 71–105.

Hansell, D. A., D. Kadko, and N. R. Bates (2004), Degradation of terrigenous dissolved organic carbon in the western Arctic Ocean, *Science*, *304*, 858–861.

Harrison, J. A., N. Caraco, and S. P. Seitzinger (2005), Global patterns and sources of dissolved organic matter export to the coastal zone: Results from a spatially explicit, global model, *Global Biogeochem. Cycles*, *19*, GB4S04, doi:10.1029/2005GB002480.

Helly, J. J., and L. A. Levin (2004), Global distribution of naturally occurring marine hypoxia on continental margins, *Deep Sea Res., Part I*, *51*(9), 1159–1168.

Humborg, C., et al. (2000), Silicon retention in river basins: Far-reaching effects on biogeochemistry and aquatic food webs in coastal marine environments, *Ambio*, *29*(1), 45–50.

Jickells, T. (1998), Nutrient biogeochemistry of the coastal zone, *Science*, *281*, 217–222.

Jickells, T. D., and L. J. Spokes (2001), Atmospheric iron inputs to the oceans, in *The Biogeochemistry of Iron in Seawater*, edited by D. R. Turner and K. A. Hunter, pp. 85–121, Wiley Intersci., New York.

Justic, D., N. N. Rabalais, and R. E. Turner (1995), Stoichiometric nutrient balance and origin of coastal eutrophication, *Mar. Pollut. Bull.*, *30*(1), 41–46.

Kalnay, E., et al. (1996), The NCEP/NCAR 40-year reanalysis project, *Bull. Am. Meteorol. Soc.*, *77*(3), 437–471.

Key, R. M., A. Kozyr, C. L. Sabine, K. Lee, R. Wanninkhof, J. L. Bullister, R. A. Feely, F. J. Millero, C. Mordy, and T.-H. Peng (2004), A global ocean carbon climatology: Results from Global Data Analysis Project (GLODAP), *Global Biogeochem. Cycles*, *18*, GB4031, doi:10.1029/2004GB002247.

Korzoun, V. I., et al. (1977), *Atlas of World Water Balance*, 36 pp., UNESCO, Paris.

Le Quéré, C., O. Aumont, P. Monfray, and J. Orr (2003), Propagation of climatic events on ocean stratification, marine biology, and CO_2: Case studies over the 1979–1999 period, *J. Geophys. Res.*, *108*(C12), 3375, doi:10.1029/2001JC000920.

Le Quéré, C., et al. (2005), Ecosystem dynamics based on plankton functional types for global ocean biogeochemistry models, *Global Change Biol.*, *11*(11), 2016–2040.

Levitus, S., et al. (1994), *World Ocean Atlas 1994*, vol. 3, *Nutrients*, *NOAA Atlas NESDIS 3*, 150 pp., U.S. Dept. of Comm., Washington, D. C.

Liu, K. K., et al. (2000), Continental margin carbon fluxes, in *The Changing Ocean Carbon Cycle: A Midterm Synthesis of the Joint Global Ocean Flux Study*, edited by R. B. Hanson et al., pp. 187–239, Cambridge Univ. Press, Cambridge.

Locarnini, R. A., et al. (2002), *World Ocean Atlas 2001*, vol. 3, *Oxygen*, in *NOAA Atlas NESDIS 51*, edited by S. Levitus, 286 pp., U.S. Gov. Print. Off., Washington, D. C.

Lohan, M. C., and K. W. Bruland (2006), Importance of vertical mixing for additional sources of nitrate and iron to surface waters on the Columbia River plume: Implications for biology, *Mar. Chem.*, *98*, 260–273.

Ludwig, W., and J. L. Probst (1998), River sediment discharge to the oceans: Present-day controls and global budgets, *Am. J. Sci.*, *298*, 265–295.

Ludwig, W., et al. (1996a), River discharges of carbon to the world's oceans: Determining local inputs of alkalinity and of dissolved and particulate organic carbon, *C. R. Acad. Sci. Ser. IIA Sci. Terres Planetes*, *323*(12), 1007–1014.

Ludwig, W., J.-L. Probst, and S. Kempe (1996b), Predicting the oceanic input of organic carbon by continental erosion, *Global Biogeochem. Cycles*, *10*(1), 23–42.

Ludwig, W., et al. (1998), Atmospheric CO_2 consumption by continental erosion: Present-day controls and implications for the last glacial maximum, *Global Planet. Change*, *17*, 107–120.

Mackenzie, F. T., et al. (1998), Role of the continental margin in the global carbon balance during the past three centuries, *Geology*, *26*(5), 423–426.

Mackenzie, F. T., et al. (2004), Boundary exchanges in the global ocean margin: Implications for the organic and inorganic carbon cycles, in *The Sea*, vol. 13, *The Global Coastal Ocean: Multiscale Interdisciplinary Processes*, edited by A. R. Robinson and K. Brink, pp. 193–226, Harvard Univ. Press, Boston.

Madec, G., et al. (1999), *OPA 8.1 Ocean General Circulation Model Reference Manual, Notes du Pole de Modelisation*, 91 pp., Inst. Pierre-Simon Laplace (IPSL), Gif-sur-Yvette, France.

Manizza, M., C. Le Quéré, A. J. Watson, and E. T. Buitenhuis (2005), Bio-optical feedbacks among phytoplankton, upper ocean physics and sea-ice in a global model, *Geophys. Res. Lett.*, *32*, L05603, doi:10.1029/2004GL020778.

Martin, J.-M., and M. Meybeck (1979), Elemental mass balance of material carried by major world rivers, *Mar. Chem.*, *7*, 173–206.

Martin, J.-M., and M. Whitfield, (1983), The significance of the river input of chemical elements to the ocean, in *Trace Metals in Sea Water*, edited by C. S. Wong et al., pp. 265–296, Plenum, New York.

Matear, R. J., and B. Elliott (2004), Enhancement of oceanic uptake of anthropogenic CO_2 by macronutrient fertilization, *J. Geophys. Res.*, *109*, C04001, doi:10.1029/2000JC000321.

McKinley, G. A., et al. (2006), North Pacific carbon cycle response to climate variability on seasonal to decadal timescales, *J. Geophys. Res.*, *111*, C07S06, doi:10.1029/2005JC003173.

Meybeck, M. (1982), Carbon, nitrogen and phosphorus transport by world rivers, *Am. J. Sci.*, *282*, 401–450.

Meybeck, M. (1998), The IGBP Water Group: A response to a growing global concern, *IGBP Global Change Newslett.*, *36*, 8–12.

Meybeck, M., and A. Ragu (Eds.) (1997), *River Discharges to the Oceans: An Assessment of Suspended Solids, Major Ions, and Nutrients*, U.N. Environ. Programme, Nairobi.

Moore, J. K., et al. (2002), Iron cycling and nutrient-limitation patterns in surface waters of the World Ocean, *Deep Sea Res., Part II*, *49*(1–3), 463.

Muller-Karger, F. E., R. Varela, R. Thunell, R. Luerssen, C. Hu, and J. J. Walsh (2005), The importance of continental margins in the global carbon cycle, *Geophys. Res. Lett.*, *32*, L01602, doi:10.1029/2004GL021346.

Paulson, C. A., and J. J. Simpson (1977), Irradiance measurements in the upper ocean, *J. Phys. Oceanogr.*, *7*, 952–956.

Rabalais, N. N., et al. (2002), Beyond science and into policy: Gulf of Mexico hypoxia and the Mississippi River, *Bioscience*, *52*, 129–142.

Reichart, G., L. J. Lourens, and W. J. Zachariasse (1998), Temporal variability in the northern Arabian Sea Oxygen Minimum Zone (OMZ) during the last 225,000 years, *Paleoceanography*, *13*(6), 607–621.

Schlitzer, R. (2002), Carbon export fluxes in the Southern Ocean: Results from inverse modeling and comparison with satellite-based estimates, *Deep Sea Res., Part II*, *49*(9–10), 1623–1644.

Schmittner, A., A. Oschlies, X. Giraud, M. Eby, and H. L. Simmons (2005), A global model of the marine ecosystem for long-term simulations: Sensitivity to ocean mixing, buoyancy forcing, particle sinking, and dissolved organic matter cycling, *Global Biogeochem. Cycles*, *19*, GB3004, doi:10.1029/2004GB002283.

Seitzinger, S. P., et al. (2002), Global patterns of dissolved inorganic and particulate nitrogen inputs to coastal systems: Recent conditions and future projections, *Estuaries*, *25*(4), 640–655.

Seitzinger, S. P., J. A. Harrison, E. Dumont, A. H. W. Beusen, and A. F. Bouwman (2005), Sources and delivery of carbon, nitrogen, and phosphorus to the coastal zone: An overview of Global Nutrient Export from Watersheds (NEWS) models and their application, *Global Biogeochem. Cycles*, *19*, GB4S01, doi:10.1029/2005GB002606.

Sholkovitz, E. R. (1978), Flocculation of Dissolved Fe, Mn, Al, Cu, Ni, Co and Cd During Estuarine Mixing, *Earth Planet. Sci. Lett.*, *41*, 77–86.

Smith, S. V., and J. T. Hollibaugh (1993), Coastal metabolism and the oceanic organic carbon balance, *Rev. Geophys.*, *31*(1), 75–89.

Smith, S. V., et al. (2003), Humans, hydrology, and the distribution of inorganic nutrient loading to the ocean, *Bioscience*, *53*, 235–245.

Takahashi, T., W. S. Broecker, and S. Langer (1985), Redfield ratio based on chemical data from isopycnal surfaces, *J. Geophys. Res.*, *90*(C10), 6907–6924.

Tegen, I., and I. Fung (1995), Contribution to the atmospheric mineral aerosol load from land surface modification, *J. Geophys. Res.*, *100*(D9), 18,707–18,726.

Treguer, P., et al. (1995), The silica balance in the world ocean: A reestimate, *Science*, *268*, 375–379.

Ukwe, C. N., et al. (2003), Achieving a paradigm shift in environmental and living resources management in the Gulf of Guinea: The large marine ecosystem approach, *Mar. Pollut. Bull.*, *47*(1–6), 219–225.

UNPD (2004), *United Nations Population Division, World Population Prospects: The 2002 Revision*, vol. III, *Analytical Report*, 347 pp., Popul. Div., Dep. of Econ. and Soc. Affairs, U.N., New York. (available at http://www.un.org/esa/population/publications/wpp2002/WPP2002_VOL_3.pdf)

Vörösmarty, C. J., et al. (2003), Anthropogenic sediment retention: Major global impact from registered river impoundments, *Global Planet. Change*, *39*(1–2), 169–190.

Wollast, R. (1998), Evaluation and comparison of the global carbon cycle in the coastal zone and in the open ocean, in *The Sea*, edited by K. Brink and A. R. Robinson, pp. 213–252, John Wiley, Hoboken, N. J.

E. T. Buitenhuis, School of Environmental Sciences, University of East Anglia, Norwich, NR4 7TJ, UK.

L. Cotrim da Cunha, Leibniz-Institut für Meereswissenschaften, Marine Biogeochemie, Düsternbrooker Weg 20, D-24105, Kiel, Germany.

X. Giraud, Research Center "Ocean Margins", University of Bremen, FB5 D-28334 Bremen, Germany.

C. Le Quéré, British Antarctic Survey, Madingley Road, Cambridge, CB3 0ET UK.

W. Ludwig, CEFREM UMR-CNRS 5110, University of Perpignan, F-66860 Cedex, Perpignan, France.